IEEE Access
Multidisciplinary ⋮ Rapid Review ⋮ Open Access Journal

Received 2 March 2024, accepted 2 May 2024, date of publication 8 May 2024, date of current version 15 May 2024.

Digital Object Identifier 10.1109/ACCESS.2024.3397655

RESEARCH ARTICLE

Performance Analysis of Modulation Strategies in Single-Phase HBNPC Inverter Across Variable Operating Conditions

NAZLICAN CAVLI[1] AND EMRE OZKOP[2], (Senior Member, IEEE)
[1]Tercan Vocational School, Erzincan Binali Yıldırım University, Erzincan, Türkiye
[2]Department of Electrical and Electronics Engineering, Karadeniz Technical University, Trabzon 61080, Türkiye
Corresponding author: Emre Ozkop (eozkop@ktu.edu.tr)

ABSTRACT This study investigates the performance of a single-phase 5-level H-Bridge Neutral Point Clamped (HBNPC) inverter across various operating conditions. These conditions encompass variations in output power, frequency, modulation index, and modulation techniques. To adapt modulation strategies typically employed in three-phase inverter structures, we apply them to a single-phase HBNPC inverter. The modulation strategies under consideration include level-shifted (LS) based on phase disposition pulse width modulation (PD-PWM), third harmonic injection pulse width modulation (THI-PWM), space vector pulse width modulation (SV-PWM), and modified PWM (MPWM). These strategies are developed using different types of reference signals (RS) and carrier signals (CS). Initially, we analyze the inverter's output voltage and current waveforms across various modulation strategy states. Subsequently, we explore the relationships between efficiency, total harmonic distortion (THD), and variable output power across different modulation strategy states. We uncover distinct patterns between modulation strategy-THD, efficiency, and output voltage for maximum inverter output power. Furthermore, we examine the relationship between the modulation index and THD for each modulation strategy state, considering different switching frequencies. Additionally, we investigate the relationship between switching frequency and THD across different modulation index values, approaching the analysis from multiple perspectives.

INDEX TERMS Multilevel inverter, modulation technique, carrier signal, HBNPC.

I. INTRODUCTION

As we continue to experience an escalating global demand for energy, the reserves of fossil fuels, which have long been our primary source of energy, are swiftly depleting. This depletion is not the only concern. The environmental impact of using such fossil fuels, such as pollution and climate change, has become increasingly apparent.

In response to these pressing issues, there is a growing trend towards the adoption of clean, eco-friendly, and renewable sources of energy. These include solar, wind, geothermal, and wave power, among others. Such sources offer a sustainable and environmentally friendly alternative to traditional fossil fuels [1], [2].

The associate editor coordinating the review of this manuscript and approving it for publication was Tariq Masood.

Among these renewable energy sources, solar energy systems have come to play a pivotal role. These systems harness energy directly from the sun, one of our most abundant natural resources, and convert it into electrical energy that can be used by consumers [3]. This process of energy production is clean, sustainable, and provides us with a virtually endless source of power.

Power electronic converters are integral components of these solar energy systems. They are used to convert the type of current and adjust the voltage in order to make the power usable in a variety of applications. Specifically, DC-DC converters and DC/AC inverters are commonly used, the selection of which depends on the specific application and location [4], [5], [6], [7].

The power quality requirements in power systems fluctuate daily in response to varying conditions [8]. Voltage

or current harmonic distortions, which detrimentally impact power quality, are predominantly generated by non-linear and switching systems. Among these systems are distributed generation units and grid-connected power electronic converters employed in reactive power and voltage compensation [9].

Inverters, as power electronic converters, are typically categorized as two-level or multilevel. Two-level inverters find common use in grid and small-scale industrial applications, whereas multilevel inverters are preferred for medium and high-power conversion scenarios [10].

Multilevel inverters offer several advantages over their two-level counterparts, including enhanced electromagnetic compatibility, greater voltage capacity, reduced switching losses, lower dv/dt, and improved power quality waveforms [11], [12]. The primary objective of multilevel inverters is to minimize harmonic distortion and produce high-quality output voltage waveforms [13], [14]. Their popularity stems from the nearly sinusoidal output waveform, which reduces the need for additional filtering [15].

However, multilevel inverters come with drawbacks such as the requirement for numerous switching elements and the potential for voltage and power imbalances [16], [17], [18]. Multilevel inverter families are typically classified into four main categories based on voltage sources: capacitor-clamped, neutral point-clamped (diode-clamped), cascaded, and hybrid multilevel inverters [19], [20].

Neutral point-clamped multilevel inverters offer advantages like reduced filtering needs due to decreased harmonic components at higher voltage levels, improved efficiency through controlled reactive power flow, and simplified control methods utilizing a back-to-back inverter system. Nonetheless, they also present challenges such as increased complexity with higher level counts, leading to reduced reliability, and difficulties in controlling active power flow [21], [22].

The capacitor-clamped inverter can theoretically accommodate infinite levels. However, practical constraints necessitate limiting it to a finite number of levels [23]. When the switch combinations in this topology are appropriately selected, the capacitor-clamped inverter can function as an active power converter [24], operating similarly to a diode-clamped inverter [25].

The primary advantages of capacitor-clamped multilevel inverters stem from auxiliary capacitors. These capacitors enable additional operation during power outages, facilitate the provision of various voltage levels through different switching states, and result in reduced harmonic distortion in the output voltage as the level increases. Consequently, there's a diminished need for additional filtering. Moreover, capacitor-clamped inverters offer the ability to control both active and reactive power [26].

However, as the inverter level increases, so does the requirement for auxiliary capacitors. This leads to increased costs due to the expensive nature of capacitors and reduces the lifetime of the inverters [27].

A cascaded H-bridge multilevel inverter comprises series-connected full-bridge inverters and, in comparison to other multilevel inverters, features fewer switching elements at the same level [18], [28]. The simplicity of its structure, ease of maintenance, minimal component count, high modularity, straightforward control, and absence of voltage balancing issues make cascaded H-bridge multilevel inverters widely preferred [29].

Increasing the inverter level enhances the output voltage quality. However, this also leads to a higher number of switching elements, resulting in increased costs, switching losses, and transmission losses, consequently reducing efficiency. Additionally, reliability decreases, and the control system becomes more complex [30], [31]. The output voltage level obtained is one phase higher than twice the number of DC sources.

Compared to other multilevel inverter topologies, cascaded H-bridge inverters require fewer switching elements for the same level, eliminating the need for additional diodes and capacitors. Their simple structure allows for scalability, modular circuit arrangement, and packaging advantages. However, a potential drawback lies in active power conversion, as it necessitates a separate asymmetrical or symmetrical DC power source for each module [32].

In modulation, the objective is to approximate the output voltage or current of the inverter to the reference signal value. Inverters can employ either current-controlled or voltage-controlled switching. However, current-controlled switching is often less favored due to its requirement for high frequencies [33].

Multilevel inverters, commonly used in applications demanding high power and voltage, operate at low frequencies. Consequently, voltage-controlled switching is prevalent in multilevel inverters as it operates at lower frequencies [34].

During the switching process, a sinusoidal signal is typically chosen as the reference signal, and a triggering signal is generated. This signal is then applied to the switching elements of the converter to derive the output signal. The chosen modulation strategy is closely intertwined with the multilevel inverter topology and significantly influences the system's performance.

The modulation strategies that are typically employed for multilevel inverters are primarily divided into two significant groups: carrier-based methods and space vector-based methods, as discussed in multiple studies [35], [36]. These methods are unique in their approach and have different usage scenarios. The carrier-based methods are typically utilized when a higher frequency is required, while space vector-based methods are used when precision is of the utmost importance. Digging deeper into the space vector-based modulation, there are additional subgroups that exist. These include the two-dimensional (2D) and three-dimensional (3D) space vector modulation methods [37]. The 2D and 3D methods are differentiated by the number of variables they can handle simultaneously,

making them more applicable in certain situations than others.

Conversely, carrier-based modulation strategies are classified based on frequency into low-frequency, medium-high-frequency, and mixed-frequency methods. Selective harmonic elimination pulse width modulation falls under the low-frequency modulation category, while hybrid pulse width modulation is categorized as a mixed-frequency method. Additionally, medium-high frequency modulation can be subdivided into phase-shifted and level-shifted modulation strategies. Examples of level-shifted modulation strategies include phase disposition, phase opposition disposition, and alternate phase opposition disposition modulation methods [38], [39].

This study is focused on evaluating the performance of a single-phase 5-level H-bridge Neutral Point Clamped (HBNPC) inverter, a critical component in many power electronics systems. The evaluation is conducted across a broad range of operating conditions, which include variations in output power levels, operating frequencies, modulation indices, and modulation techniques. The purpose is to gain a more nuanced understanding of the inverter's capabilities and limitations.

Modulation strategies, which are typically deployed in three-phase inverter setups, are adapted and implemented in the single-phase HBNPC inverter for this study. These strategies are multifarious and encompass a range of techniques including level-shifted (LS) phase disposition pulse width modulation (PD-PWM), third harmonic injection pulse width modulation (THI-PWM), space vector pulse width modulation (SV-PWM), and a modified version of PWM (MPWM).

Each of these strategies utilizes distinct types of reference signals (RS) and carrier signals (CS). The selection of these signals plays a crucial role in the performance of the inverter and the quality of the output power. The comparative analysis of these various modulation strategies provides valuable insights into their respective merits and shortcomings, thereby enabling more informed decisions regarding their applicability in different scenarios.

II. METHOD

A. TOPOLOGY

This study entails simulation studies on a 5-level H-bridge Neutral Point Clamped (HBNPC) inverter. Figure 1 illustrates the circuit diagram of the 5-level HBNPC inverter [40]. This inverter comprises two half-bridge arms with three-level diode clamps. The combination of each three-level diode-clamped inverter, with output voltages of $+V_{dc}/2$, 0, $-V_{dc}/2$ forms a five-level output voltage inverter with $+V_{dc}$, $+V_{dc}/2$, 0, $-V_{dc}/2$ ve $-V_{dc}$. The switching states of the five-level HBNPC inverter depicted in Figure 1 are detailed in Table 1.

Selective harmonic elimination pulse width modulation (SHE-PWM), sinusoidal pulse width modulation (SPWM), and space vector pulse width modulation (SV-PWM) are techniques applicable to a 5-level H-Bridge Neutral Point Clamped (HBNPC) inverter. Notably, this topology has been successfully commercialized for medium voltage three-phase motor drives by ABB and TMEIC-GE [41].

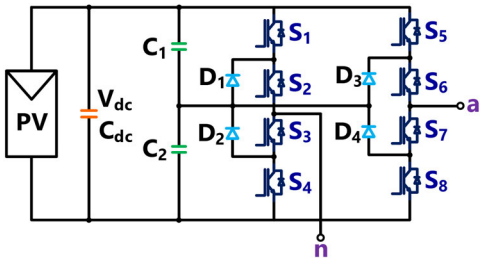

FIGURE 1. 5-level HBNPC inverter circuit diagram.

TABLE 1. 5-level HBNPC inverter switching states.

V_{an}	S_1	S_2	S_3	S_4	S_5	S_6	S_7	S_8
$+V_{dc}$	OFF	OFF	ON	ON	ON	ON	OFF	OFF
$+V_{dc}/2$	OFF	ON	ON	OFF	ON	ON	OFF	OFF
	OFF	OFF	ON	ON	OFF	ON	ON	OFF
0	ON	ON	OFF	OFF	ON	ON	OFF	OFF
	OFF	ON	ON	OFF	OFF	ON	ON	OFF
	OFF	OFF	ON	ON	OFF	OFF	ON	ON
$-V_{dc}/2$	ON	ON	OFF	OFF	OFF	ON	ON	OFF
	OFF	ON	ON	OFF	OFF	OFF	ON	ON
$-V_{dc}$	ON	ON	OFF	OFF	OFF	OFF	ON	ON

B. MODULATION TECHNIQUE

1) SPWM TECHNIQUE

One of the most widely used modulation techniques in multilevel inverters is Sinusoidal Pulse Width Modulation (SPWM). In SPWM, the pulse widths applied vary based on the amplitude of the sine wave, resulting in significantly reduced distortion factors and lowest-order harmonics. To adapt SPWM for multilevel inverter topologies, multiple carriers are utilized, leading to the development of multi-carrier PWM methods.

Two examples of multi-carrier PWM methods are Phase-Shifted Pulse Width Modulation (PS-PWM) and Level-Shifted Pulse Width Modulation (LS-PWM). In LS-PWM, the carrier signals can be amplitude-shifted relative to each other and to each possible output voltage level generated by the inverter.

Based on the triangular waveform structure, three different types of switching signals can be generated: Phase Disposition (PD), Phase Opposition Disposition (POD), and Alternate Phase Opposition Disposition (APOD) [42]. In this study, the PD-PWM method is employed, as illustrated in Figure 2.

To delve into the subject, we provide the equations for the pertinent carrier and modulation signals below:

$$C_x(t) = f_x(t) = \frac{2A}{T}\left|t - T\left\lfloor \frac{t}{T} + \frac{1}{2}\right\rfloor\right| \tag{1}$$

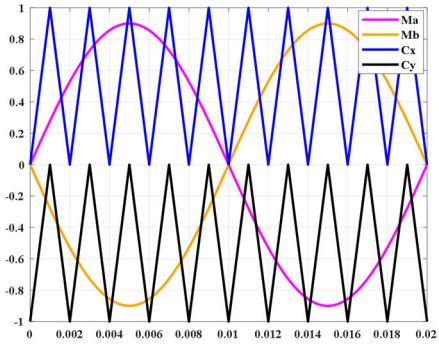

FIGURE 2. LS-based PD-PWM method.

$$C_y(t) = f_y(t) = \frac{2A}{T}\left|t - T\left\lfloor \frac{t}{T} + \frac{1}{2}\right\rfloor\right| - A \quad (2)$$

$$M_a(t) = f_a(t) = A\sin\left(2\pi\frac{1}{T}t\right) \quad (3)$$

$$M_b(t) = f_b(t) = A\sin\left(2\pi\frac{1}{T}t + \pi\right) \quad (4)$$

where A is maximum amplitute, T is period and t is time.

2) THI-PWM TECHNIQUE

The research findings indicate that augmenting the target reference waveform of each phase leg with a common mode n-th harmonic term can enhance the maximum modulation index of the three-phase PWM inverter system [43]. Utilizing the Third Harmonic Injection Pulse Width Modulation (THI-PWM) method enables an increase in the maximum achievable output voltage value. The equations representing the fundamental modulation signal (V_m), the third harmonic component of the fundamental modulation signal ($V_{m/n}$), and the combination of these two signals ($V_{(m+m/n)}$) are provided below.

$$V_m = m_{index}V_{dc}\sin\omega_0 t \quad (5)$$

$$V_{m/n} = m_{index-3}V_{dc}\sin 3\omega_0 t \quad (6)$$

$$V_{(m+m/n)} = V_{dc}(m_{index}sin\omega_0 t + m_{index-3}\sin 3\omega_0 t) \quad (7)$$

After conducting the analyses, it has been determined that the modulation index m_{index} can be increased up to a value of $2/\sqrt{3} = 1.15$, and accordingly, the modulation index $m_{index-3}$ can reach a value of $\sqrt{3}/9 = 0.192$. Different values of the modulation index $m_{index-3}$ can alter the characteristics of the inverter output [44].

In three-phase systems, the third harmonic output voltage is not visually discernible. Waveforms illustrating the time-dependent variations of the modulation signals, as expressed in Equations 5-7, are depicted in Figure 3.

The THD values obtained using the THI-PWM method in single-phase inverter topologies tend to be higher compared to those in three-phase inverter topologies. This disparity arises because, in three-phase THI-PWM, the third harmonic components in all phases align in the same phase, effectively canceling each other out. Consequently, the application of

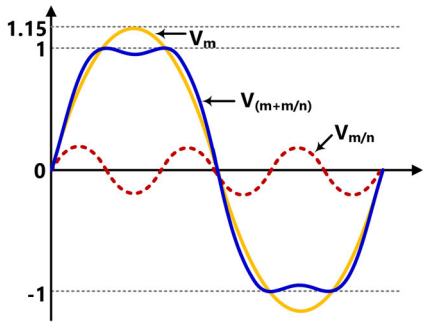

FIGURE 3. THI-PWM method basic modulation signals.

THI-PWM in single-phase systems often falls short of the anticipated results in terms of THD.

In the realm of three-phase inverter topologies, the THI-PWM method stands out as it has been found to achieve a higher output in terms of voltage and current, while simultaneously maintaining lower THD values when compared to other PWM methods [45]. In this study, one of the modulation techniques employed is the THI-PWM method. Specifically, the LS-based Phase Disposition THI-PWM (PD-THI-PWM) method is utilized for a single-phase 5-level HBNPC inverter system, and the waveform representing this method is illustrated in Figure 4.

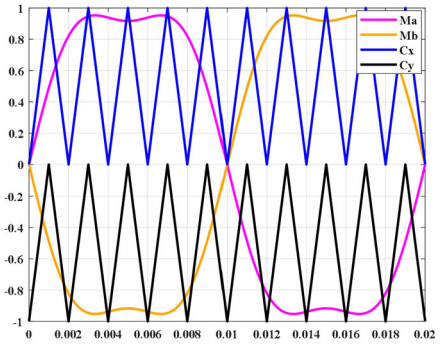

FIGURE 4. LS-based PD-THI-PWM method.

3) SV-PWM TECHNIQUE

In single-phase systems, the implementation of Space Vector Pulse Width Modulation (SV-PWM) differs from that in three-phase systems. Depending on the characteristics of the power electronic converter to be employed, it becomes necessary to readjust the structure of SV-PWM. In the context of this study, the initial step in utilizing SV-PWM as the modulation technique for controlling the single-phase 5-level HBNPC inverter, as discussed and illustrated in Figure 1, involves determining the inverter's operating modes. These operating modes are depicted in Figure 5 [46].

The working conditions of these operating modes are outlined in Table 2. The inverter output voltage is constrained within the limits of V_{an}, 0, $\mp V_{dc}/2$ ve $\mp V_{dc}$ values [47]. To ensure the desired modulation reference sinusoidal voltage

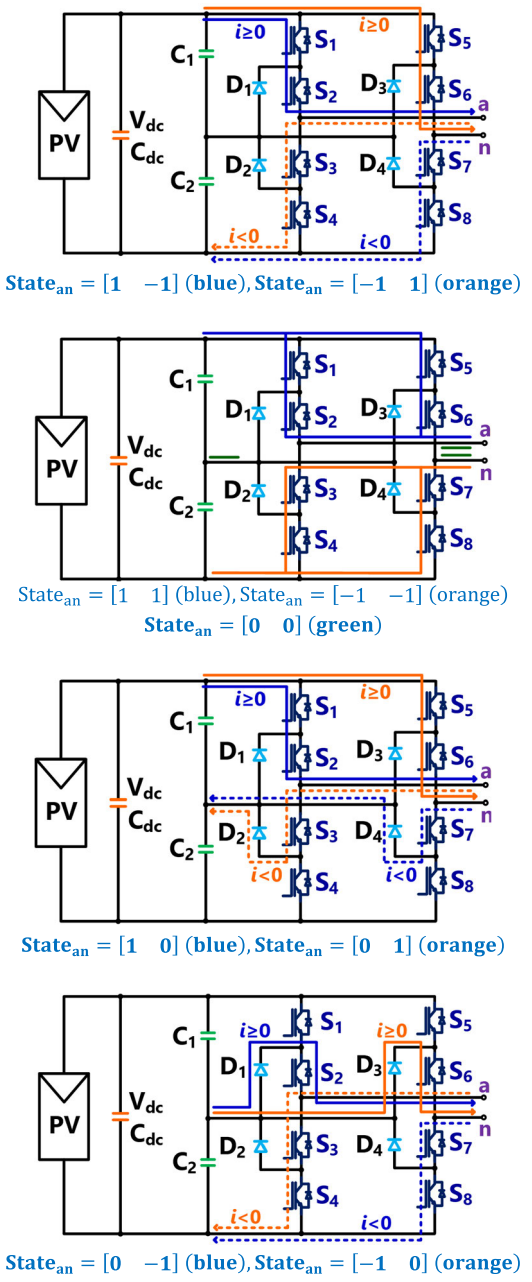

FIGURE 5. Simplified operating modes for a single-phase 5-level HBNPC inverter.

waveform (v_{ref}) at the output, the switching process must adhere to a specific sequence during operation. Figure 6 illustrates the resultant waveforms of the observed inverter output voltage and modulation reference voltage signal [48].

The modulation reference voltage signal can be expressed as follows.

$$v_{ref} = m_{index} \sin(\omega t + \theta) \tag{8}$$

Here, m_{index} is the modulation index, and θ is the initial phase of v_{ref}.

As depicted in Figure 6, the stationary coordinate frame can be divided into four sectors, each determined by the value

TABLE 2. Operating conditions for a single-phase 5-level HBNPC inverter.

State	Vec.	S_1	S_2	S_3	S_4	S_5	S_6	S_7	S_8	Ph.-a	Ph.-n	V_{an}
[1 1]	$V_{1,1}$	1	1	0	0	1	1	0	0	$V_{dc}/2$	$V_{dc}/2$	0
[1 0]	$V_{1,0}$	1	1	0	0	0	1	1	0	$V_{dc}/2$	0	$V_{dc}/2$
[1 −1]	$V_{1,-1}$	1	1	0	0	0	0	1	1	$V_{dc}/2$	$-V_{dc}/2$	V_{dc}
[0 1]	$V_{0,1}$	0	0	1	1	1	1	0	0	0	$V_{dc}/2$	$-V_{dc}/2$
[0 0]	$V_{0,0}$	0	1	1	0	0	1	1	0	0	0	0
[0 −1]	$V_{0,-1}$	0	1	1	0	0	0	1	1	0	$-V_{dc}/2$	$V_{dc}/2$
[−1 1]	$V_{-1,1}$	0	0	1	1	1	1	0	0	$-V_{dc}/2$	$V_{dc}/2$	$-V_{dc}$
[−1 0]	$V_{-1,0}$	0	0	1	1	0	1	1	0	$-V_{dc}/2$	0	$-V_{dc}/2$
[−1 −1]	$V_{-1,-1}$	0	0	1	1	0	0	1	1	$-V_{dc}/2$	$-V_{dc}/2$	0

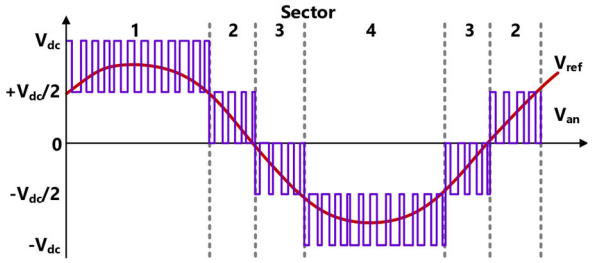

FIGURE 6. Sectors for SVPWM technique.

of v_{ref} [49].

$$\text{Sector-1: } 0.5 \leq v_{ref} \leq 1 \tag{9}$$

$$\text{Sector-2: } 0 \leq v_{ref} < 0.5 \tag{10}$$

$$\text{Sector-3: } -0.5 < v_{ref} < 0 \tag{11}$$

$$\text{Sector-4: } -1 \leq v_{ref} \leq -0.5 \tag{12}$$

The working situations related to these sectors are provided below.

Sector-1:

$$State_{an} = \{[1\ 0], [1\ -1], [1\ 0]\} \tag{13}$$

Sector-2:

$$State_{an} = \{[1\ 0], [0\ 0], [1\ 0]\} \tag{14}$$

Sector-3:

$$State_{an} = \{[-1\ 0], [0\ 0], [-1\ 0]\} \tag{15}$$

Sector-4:

$$State_{an} = \{[-1\ 0], [-1\ 1], [-1\ 0]\} \tag{16}$$

As the modulation reference voltage signal (v_{ref}) remains constant throughout one switching period (T_s), the vectors in the corresponding sector are active during specific operating time intervals. Notably, two vectors (V_1 and V_2) perform their tasks in their respective time intervals (T_1 and T_2) during one switching period (T_s), leading to the following equations.

$$V_{an}T_s = V_1T_1 + V_2T_2 \tag{17}$$

$$T_s = T_1 + T_2 \tag{18}$$

The operating time intervals of the output voltage vectors can be selected based on the sectors, as illustrated in Table 3. Numerous studies in literature have explored the number and value of these operating time intervals. Increasing the number of intervals is noted to reduce system losses and decrease THD values. Specifically, in sector structures characterized by symmetries, adjusting the time intervals in symmetry sectors compared to other symmetric sectors has been observed to positively influence system performance.

TABLE 3. Output voltage vectors during operating time interval.

Sector \ Time	T_1	T_2
1	$2(V_{dc}-u_\alpha)\,T_s/V_{dc}$	$(2u_\alpha-V_{dc})\,T_s/V_{dc}$
2	$2u_\alpha\,T_s/V_{dc}$	$(V_{dc}-2u_\alpha)\,T_s/V_{dc}$
3	$-2u_\alpha\,T_s/V_{dc}$	$(V_{dc}+2u_\alpha)\,T_s/V_{dc}$
4	$2(V_{dc}+u_\alpha)\,T_s/V_{dc}$	$-(V_{dc}+2u_\alpha)\,T_s/V_{dc}$

4) MPWM TECHNIQUE

In addition to traditional space vector and carrier-based fundamental modulation techniques, a wide range of hybrid and modified modulation techniques have been explored in the academic literature for multilevel inverters. These innovative techniques, often derived from a strategic combination of traditional space vector and carrier-based methods, offer the potential for enhanced performance and more robust control.

One key characteristic of these hybrid and modified modulation techniques is that they typically involve careful variations in the carrier signal used during the modulation process. These variations can be adjusted and optimized to suit specific system requirements and operational contexts, opening up a wide range of potential applications and use cases.

This particular study places a specific emphasis on the application of a modified Pulse Width Modulation technique, also known as MPWM. This technique is based on the concept of level-shifted carrier signal shapes and is applied using single and two-loop carrier rotation structures. The choice of these specific carrier rotation structures is strategic and is designed to maximize the performance and efficiency of the multilevel inverter system.

These advanced modulation techniques are implemented on a single-phase 5-level HBNPC inverter. The specific design and configuration of this inverter, as well as the application of the aforementioned modulation techniques, are illustrated in detail in Figure 7. This figure provides a comprehensive view of the system, offering valuable insights into its operation and performance.

The equations related to the carrier signals are given below:

$$CS_{single-loop(ps)}(t) = f_{cs-single-loop(positive)}(t) = \begin{cases} \frac{2A}{T}\left|t-\frac{T}{2}\left\lfloor\frac{2t}{T}+\frac{1}{2}\right\rfloor\right|+0 & 0\le t<T/2 \\ \frac{2A}{T}\left|t-\frac{T}{2}\left\lfloor\frac{2t}{T}+\frac{1}{2}\right\rfloor\right|+\frac{A}{2} & T/2\le t<T \end{cases} \tag{19}$$

$$CS_{single-loop(ng)}(t) = f_{cs-single-loop(negative)}(t) = \begin{cases} \frac{2A}{T}\left|t-\frac{T}{2}\left\lfloor\frac{t}{T}+\frac{1}{2}\right\rfloor\right|-\frac{A}{2} & 0\le t<T/2 \\ \frac{2A}{T}\left|t-\frac{T}{2}\left\lfloor\frac{t}{T}+\frac{1}{2}\right\rfloor\right|-A & T/2\le t<T \end{cases} \tag{20}$$

$$CS_{two-loop(ps)}(t) = f_{cs-two-loop(positive)}(t) = \begin{cases} \frac{4A}{T}\left|t-\frac{T}{4}\left\lfloor\frac{4t}{T}+\frac{1}{2}\right\rfloor\right|+5 & 0\le t<T/2 \\ \frac{4A}{T}\left|t-\frac{T}{4}\left\lfloor\frac{4t}{T}+\frac{1}{2}\right\rfloor\right|+\frac{A}{2} & T/2\le t<T \end{cases} \tag{21}$$

$$CS_{two-loop(ng)}(t) = f_{cs-two-loop(negative)}(t) = \begin{cases} \frac{4A}{T}\left|t-\frac{T}{4}\left\lfloor\frac{4t}{T}+\frac{1}{2}\right\rfloor\right|-A & 0\le t<T/2 \\ \frac{4A}{T}\left|t-\frac{T}{4}\left\lfloor\frac{4t}{T}+\frac{1}{2}\right\rfloor\right|-\frac{A}{2} & T/2\le t<T \end{cases} \tag{22}$$

where A is maximum amplitude, T is period, and t is time.

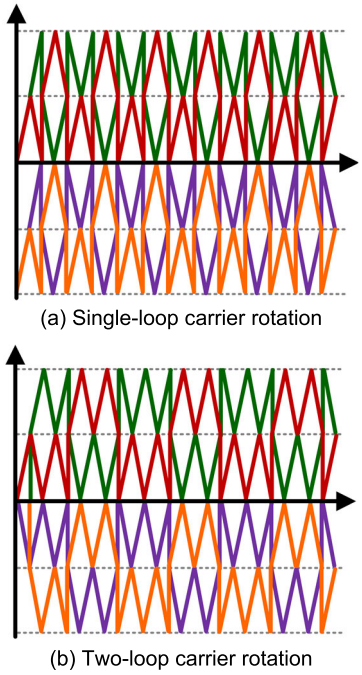

FIGURE 7. Modified carrier signals for the MPWM technique.

5) SIGNAL GENERATION

The fundamental block diagram of the standalone single-phase 5-level HBNPC inverter system is illustrated in Figure 8. This diagram includes a pivotal component known as the signal generation block. The function of this critical block is to generate the switching strategy, which is an integral part of the system's operation. The switching strategy is responsible for determining which switches within the

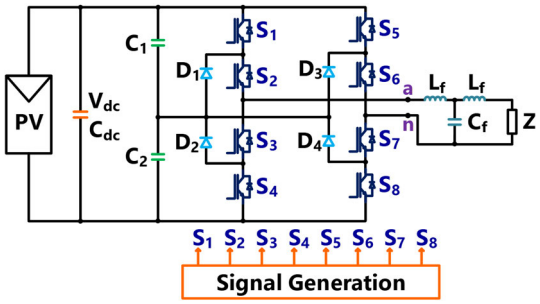

FIGURE 8. Standalone inverter system basic circuit block diagram.

system will be activated (ON) or deactivated (OFF). It also establishes the sequence and frequency of these actions. The determination is based on a variety of factors, including the inverter topology, the reference signal, and the carrier signal. To provide a clearer understanding, Figure 9 presents an in-depth block diagram of the signal generation block that was used in the simulation study. Figure 9.a is employed for the SPWM, THI-PWM, MPWM techniques, serving as a visual representation of these techniques' signal generation. On the other hand, Figure 9.b is utilized for the SV-PWM technique in generating the switching signal, offering a detailed schematic of this specific method.

The types and waveforms of the Reference Signal (RS) and Carrier Signal (CS) specified in the signal generation block, as depicted in Figure 9, vary depending on the modulation technique to be applied. Detailed illustrations of the RS and CS types and waveforms can be found in Figures 10 and 11, respectively.

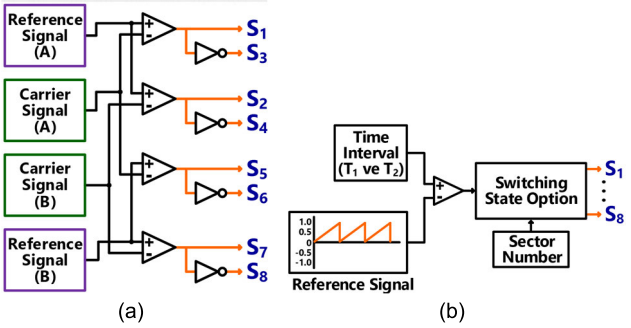

FIGURE 9. Signal generation basic circuit block diagram.

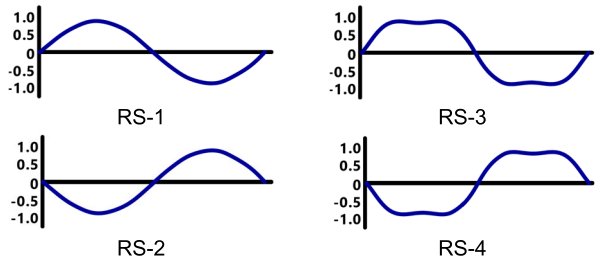

FIGURE 10. The RS types/waveforms.

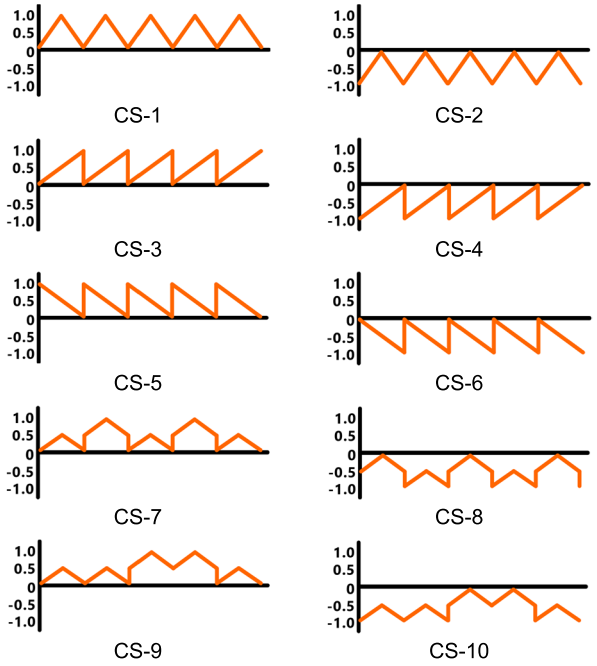

FIGURE 11. The CS types/waveforms.

The equations related to the CS types/waveforms are given below:

$$CS_1(t) = f_{CS-1}(t) = \frac{2A}{T}\left|t - T\left\lfloor \frac{t}{T} + \frac{1}{2}\right\rfloor\right| \tag{23}$$

$$CS_2(t) = f_{cs-2}(t) = \frac{2A}{T}\left|t - T\left\lfloor \frac{t}{T} + \frac{1}{2}\right\rfloor\right| - A \tag{24}$$

$$CS_3(t) = f_{cs-3}(t) = \frac{A}{T}\left(\left(t - \frac{T}{2}\right) - T\left\lfloor \frac{t - T/2}{T} + \frac{1}{2}\right\rfloor\right) + \frac{A}{2} \tag{25}$$

$$CS_4(t) = f_{cs-4}(t) = \frac{A}{T}\left(\left(t - \frac{T}{2}\right) - T\left\lfloor \frac{t - T/2}{T} + \frac{1}{2}\right\rfloor\right) - \frac{A}{2} \tag{26}$$

$$CS_5(t) = f_{cs-5}(t) = \frac{A}{T}\left(-\left(t - \frac{T}{2}\right) - T\left\lfloor \frac{-(t - T/2)}{T} + \frac{1}{2}\right\rfloor\right) + \frac{A}{2} \tag{27}$$

$$CS_6(t) = f_{cs-6}(t) = \frac{A}{T}\left(-\left(t - \frac{T}{2}\right) - T\left\lfloor \frac{-(t - T/2)}{T} + \frac{1}{2}\right\rfloor\right) - \frac{A}{2} \tag{28}$$

$$CS_7(t) = f_{cs-7}(t) = \begin{cases} \frac{2A}{T}\left|t - \frac{T}{2}\left\lfloor \frac{2t}{T} + \frac{1}{2}\right\rfloor\right| + 0 & 0 \le t < T/2 \\ \frac{2A}{T}\left|t - \frac{T}{2}\left\lfloor \frac{2t}{T} + \frac{1}{2}\right\rfloor\right| + \frac{A}{2} & T/2 \le t < T \end{cases} \tag{29}$$

$$CS_8(t) = f_{cs-8}(t) = \begin{cases} \frac{2A}{T}\left|t - \frac{T}{2}\left\lfloor \frac{t}{T} + \frac{1}{2}\right\rfloor\right| - \frac{A}{2} & 0 \le t < T/2 \\ \frac{2A}{T}\left|t - \frac{T}{2}\left\lfloor \frac{t}{T} + \frac{1}{2}\right\rfloor\right| - A & T/2 \le t < T \end{cases} \quad (30)$$

$$CS_9(t) = f_{cs-9}(t) = \begin{cases} \frac{4A}{T}\left|t - \frac{T}{4}\left\lfloor \frac{4t}{T} + \frac{1}{2}\right\rfloor\right| + 5 & 0 \le t < T/2 \\ \frac{4A}{T}\left|t - \frac{T}{4}\left\lfloor \frac{4t}{T} + \frac{1}{2}\right\rfloor\right| + \frac{A}{2} & T/2 \le t < T \end{cases} \quad (31)$$

$$CS_{10}(t) = f_{cs-10}(t) = \begin{cases} \frac{4A}{T}\left|t - \frac{T}{4}\left\lfloor \frac{4t}{T} + \frac{1}{2}\right\rfloor\right| - A & 0 \le t < T/2 \\ \frac{4A}{T}\left|t - \frac{T}{4}\left\lfloor \frac{4t}{T} + \frac{1}{2}\right\rfloor\right| - \frac{A}{2} & T/2 \le t < T \end{cases} \quad (32)$$

where A is maximum amplitude, T is period, and t is time.

The signal generation block depicted in Figure 9 outlines the type and waveform details of CS and RS applicable for the SPWM, THI-PWM, and MPWM techniques. These details are summarized in Table 4.

TABLE 4. State, modulation technique, RS and CS type matric.

State	Modulation Technique	Reference Signal (RS)		Carrier Signal (CS)	
		A	B	A	B
I	SPWM	RS-1	RS-2	CS-3	CS-4
II	SPWM	RS-1	RS-2	CS-5	CS-6
III	SPWM	RS-1	RS-2	CS-1	CS-2
IV	THI-PWM	RS-3	RS-4	CS-3	CS-4
V	THI-PWM	RS-3	RS-4	CS-5	CS-6
VI	THI-PWM	RS-3	RS-4	CS-1	CS-2
VIII-a	MPWM-I	RS-1	RS-2	CS-7	CS-8
VIII-b	MPWM-I	RS-1	RS-2	CS-9	CS-10

C. FILTER

Renewable energy sources necessitate power electronic converters to efficiently transfer energy to the grid. These converters employ PWM techniques during the switching process, resulting in the presence of harmonic components in the output voltage. To prevent issues stemming from the injection of harmonic current into the grid, it becomes imperative to filter the output voltage. The integration of filters in grid-connected systems is essential for mitigating voltage harmonics and ensuring adherence to grid-connection standards for the converter.

The basic LCL filter circuit diagram, depicted in Figure 12, consists of one capacitor and two inductors. As the number of elements increases, their values tend to decrease. This type of filter exhibits the highest attenuation at high frequencies and is particularly effective in reducing harmonics. However, it is prone to resonance and is more complex to design compared to other filters. Despite its complexity, the LCL filter is adept at handling sudden discharge currents due to its inductive output. The values of capacitors and inductors for the LCL filter are determined using specific equations [50].

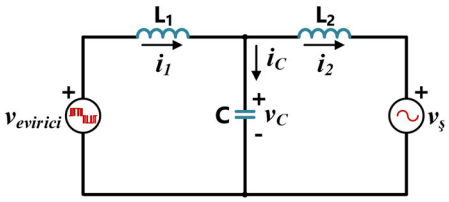

FIGURE 12. Basic LCL filter circuit schema.

$$L_{1\_min} \ge \frac{1}{8}\frac{V_{in}}{I_1}\frac{T_{sw}}{\lambda_{c_{L1}}}, \quad 20\% \le \lambda_c \le 30\% \quad (33)$$

$$L_{1\_max} \le \frac{V_{\S}}{I_1}\frac{\lambda_{c\_L1}}{\omega_0}, \quad \lambda_c \cong 5\% \quad (34)$$

$$C \le \frac{P_o}{V_{\S}^2}\frac{\lambda_c}{\omega_o}, \quad \lambda_c \cong 5\% \quad (35)$$

$$L_2 \le \left(\frac{1}{\omega_h^2 - 1}\right)\left(\frac{1}{L_1 C}\right)\cdot\left(\frac{1}{\omega_h \lambda_h I_2}\left(\omega_h \lambda_h I_2 L_1 + |V_{inv}(j\omega_h)|\right)\right) \quad (36)$$

In the above equations, the symbols represent the following parameters: V_{in} is the input voltage of the inverter, T_{sw} is the carrier period, I_1 is the inductance current, λ_{c_L1} is the fluctuation constant, V_g is the grid voltage, ω_0 is the angular frequency of the modulation signal, λ_c is the ratio of the reactive power generated by the filter capacitance to the nominal output active power of the grid-connected converter, P_o is the nominal output active power of the grid-connected inverter, V_{inv} is the output voltage of the inverter, I_2 is the injected grid current, λ_h is the harmonic ratio of the dominant harmonic, ω_h is the angular frequency of the dominant harmonic and f_h is the dominant harmonic frequency.

III. SIMULATION

In this section of the study, simulations will be conducted to evaluate various modulation techniques in a single-phase 5-level HBNPC inverter. The objective is to assess the inverter's performance under different operating conditions. This will involve observing the waveforms of the inverter output current and voltage to analyze the effects of different modulation techniques.

Furthermore, the efficiency of the inverter, including Normal efficiency, European efficiency, and California efficiency, will be evaluated. Additionally, the active inverter input and output powers, as well as THD values, will be calculated.

The study will delve into the intricate relationship between output power, THD, and efficiency in relation to the

modulation technique used in an inverter. This involves a comprehensive exploration of how these variables interact and affect one another. Moreover, the research will also investigate the correlation between the modulation index, the switching frequency, THD, and the output voltage of the inverter, which is a relationship that is crucial to understanding the overall performance of the inverter system.

In order to conduct this comprehensive similarity study, the study will employ the general block diagram of the single-phase 5-level HBNPC inverter system, as depicted in Figure 8. This diagram serves as an essential blueprint for understanding the system's operations.

The generated switching signals found within the Signal Generation block are then transmitted to the corresponding inverter switches, labeled as S_1 through S_8. These signals, which are guided by a strategically appropriate switching strategy, are responsible for producing the output voltage of the inverter. Following this, the voltage output then travels through a filter, which serves to ensure the smooth flow of current, before finally reaching the connected load. This process provides a clear demonstration of the operation of an inverter system and the factors that influence its performance.

A. TEST-I

This section will demonstrate the relationship between output power, THD, and efficiency concerning the inverter modulation technique through simulation studies. The modulation techniques to be applied, along with the types of carrier signals, are outlined in Table 5, while Table 6 provides the parameter values for the system simulation.

TABLE 5. Modulation techniques and CS types for simulation study.

Modulation Technique	CS Type	State
SPWM	Right-leaning saw	I
	Left-leaning saw	II
	Triangle	III
THI-PWM	Right-leaning saw	IV
	Left-leaning saw	V
	Triangle	VI
SV-PWM		VII
MPWM-I		VIII-a
MPWM-II		VIII-b

This study aims to investigate the impact of different modulation techniques on the system outputs. The adjustment of the output load (R_{Load}) value enables control over the system's output power. By measuring the current and voltage at specific points, the converter input power (P_{input}), output power (P_{output}),, and essential efficiency of the inverter (η), European efficiency (η_{Europe}), California efficiency ($\eta_{California}$), and THD related to the output current can be calculated.

The essential efficiency, European efficiency, and California efficiency of the inverter are defined by the following equations [51]:

TABLE 6. System simulation parameters.

DC Source		Inverter	
V_{dc}	400 V	P	4.0 kW
Filter		$C_1 = C_2$	1.65 mF
L_f	3.0 mH	Switch- Diode	
C_f	2.2 µF	R_{on}	1.1 mΩ
Load		L_{on}	0.0 mH
R_L	0-500 Ω	V_F	1.5 V
Modulation Info.			
f_{sw}	20 kHz	m_{index}	0.9

$$\eta = 100 \times (P_{input}/P_{output}) \tag{37}$$

$$\eta_{Europe} = \frac{1}{100}[3 \times \eta_{5\%} + 6 \times \eta_{10\%} + 13 \times \eta_{20\%} + 10 \times \eta_{30\%} + 48 \times \eta_{50\%} + 20 \times \eta_{100\%}] \tag{38}$$

$$\eta_{California} = \frac{1}{100}[4 \times \eta_{10\%} + 5 \times \eta_{20\%} + 12 \times \eta_{30\%} + 21 \times \eta_{50\%} + 53 \times \eta_{75\%} + 5 \times \eta_{100\%}] \tag{39}$$

In our research, a detailed simulation study was carried out. The parameters of this study were carefully controlled, keeping the input voltage (V_{input}), the switching frequency (f_{sw}), and the modulation index (m_{index}) constant throughout. Meanwhile, the output load (R_{Load}) was the variable that was allowed to change during the course of the simulation. This design was chosen to closely examine the impact of varying output load on the overall performance of the system. As shown in Figure 13, the waveforms of the inverter output voltage, the load current, and the voltage are all depicted at the maximum value of the inverter output power (P_{output}). These are shown for all states, from State-I to State-VIII, providing a comprehensive view of the system's functioning under different conditions.

When we closely examine the output voltage waveforms of the inverter as presented in Figure 13, specifically within the time interval of t = 0.16 − 0.17 ms, we can clearly identify the existence of distinct boundary regions. These boundary regions range from $[0 - V_{dc}/2 - V_{dc} - V_{dc}/2 - 0]$. The aspect worth noting here is that the time interval corresponding to the $[V_{dc}/2 - V_{dc} - V_{dc}/2]$ value range is considerably narrower for State-I, II, III, VII, and VIII-b (as shown in Figure 13 (a), (b), (c), (g), and (i)) when compared to State-IV, V, VI, and VIII-a (as shown in Figure 13 (d), (e), (f), and (h)), respectively.

Figure 13 serves as a visual representation, illustrating that the waveforms of the load voltage and current exhibit a striking structural similarity, and importantly, without any observable phase difference. This observed phenomenon can be attributed to the resistive nature of the load. When we put into application the THI-PWM modulation technique with various carrier signals (as shown in Figure 13 (d)-(f)), the outcome is that the waveforms of the load voltage and current deviate significantly from a pure sinusoid. In contrast, when

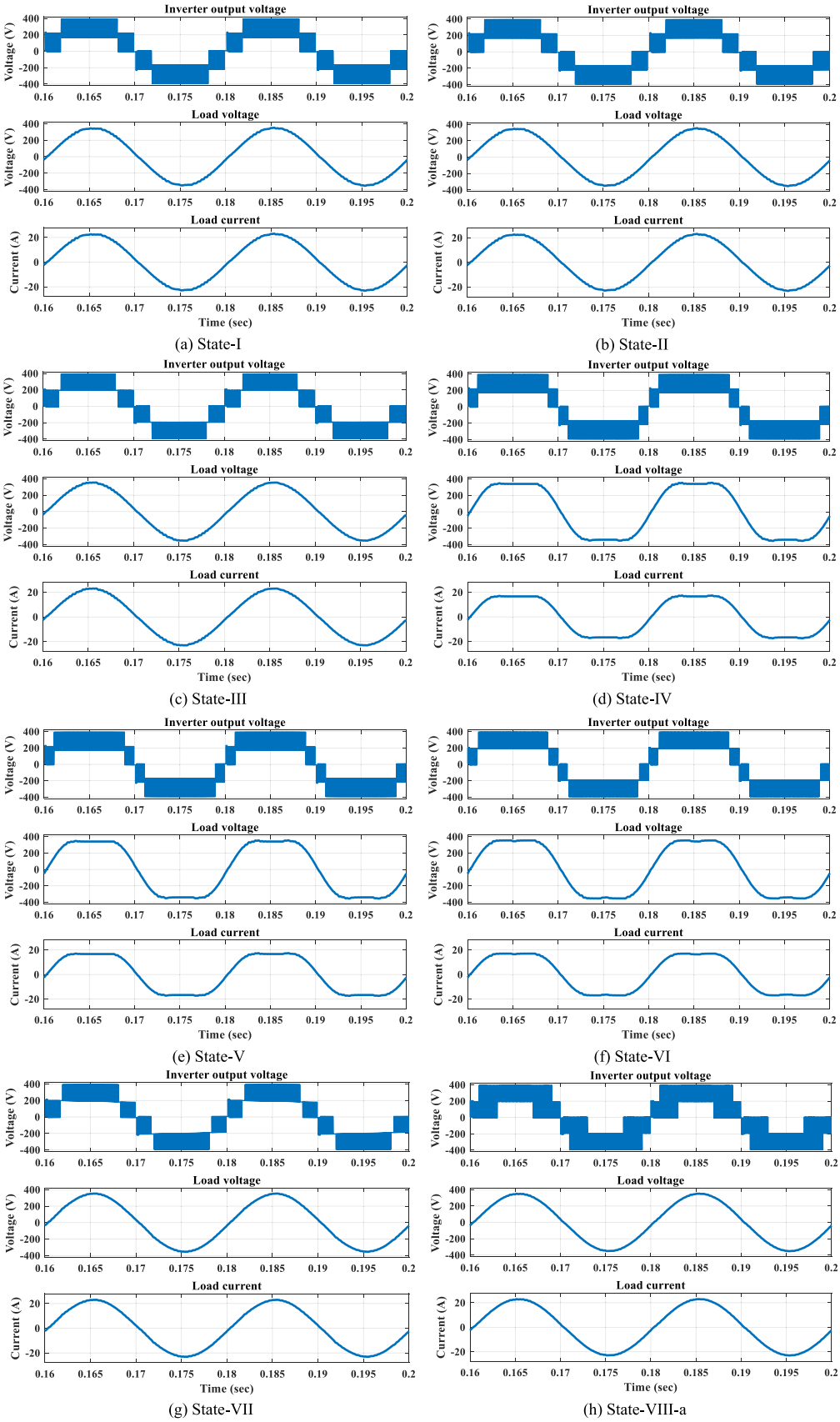

FIGURE 13. Results for voltage and current waveforms.

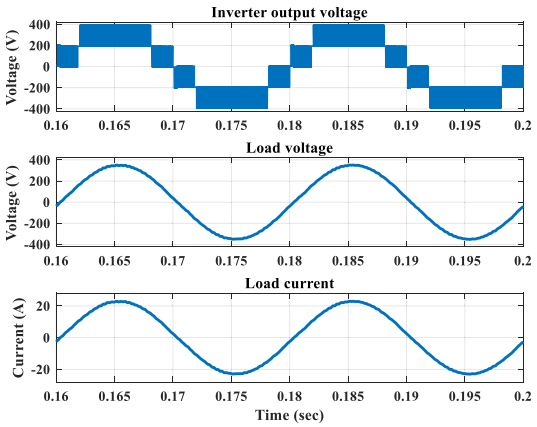

(i) State-VIII-b

FIGURE 13. *(Continued.)* **Results for voltage and current waveforms.**

the SPWM, SV-PWM, and MPWM techniques are employed (as shown in Figure 13 (a)-(c), (g)-(i)), the waveforms of the load voltage and current bear a close resemblance to a pure sinusoidal waveform.

In the context of three-phase multilevel inverter applications that utilize the THI-PWM technique, the third harmonic components in all phases neutralize each other due to their phase alignment. However, in the single-phase inverter topology that is considered in this study (as shown in Figure 13 (d)-(f)), an output current and voltage with a third harmonic are noticeably observed.

Lastly, the variations in power and efficiency across the simulated states, as well as the changes in THD and efficiency, are graphically represented in Figures 14 and 15, respectively.

The examination conducted on States-I and II, as well as States-IV and V, showed that they produced similar results. As a result of this similarity, the results for States-II and V are omitted from Figures 14 and 15, to avoid redundancy.

Moving on to the investigation of a single-phase 5-level HBNPC inverter, it was found that there were consistent efficiency variations concerning the output power. These variations were observed for different modulation techniques and different types of carrier signals. These findings are clearly illustrated in Figure 14 for better understanding.

It is worth noting that there is a noticeable correlation between the inverter output power and both efficiency (as seen in Figure 14) and THD (as seen in Figure 15). As the inverter output power increases, the efficiency and THD both demonstrate a trend of decrease.

In a more detailed observation, it was found that States-IV and VI, which employ the THI-PWM technique, show significantly higher THD values than other states. This is an important observation as it shows the impact of the THI-PWM technique on THD values.

Finally, a comparative analysis was conducted on SPWM, THI-PWM, SV-PWM, and MPWM techniques. This comparative analysis was done across different states and the results

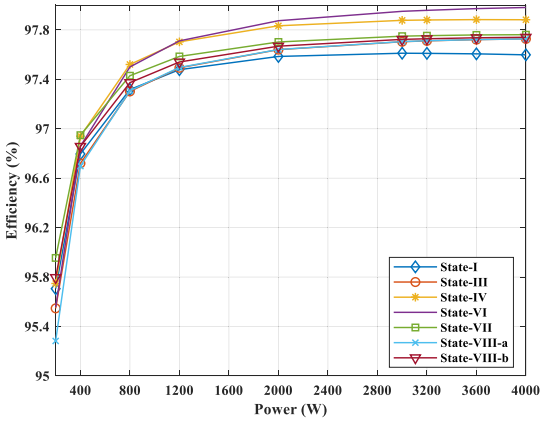

FIGURE 14. **Efficiency-power.**

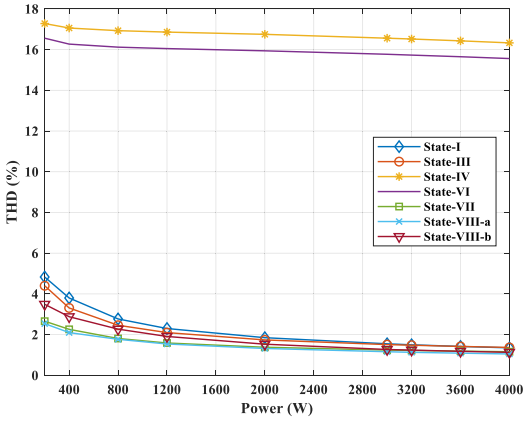

FIGURE 15. **THD-power.**

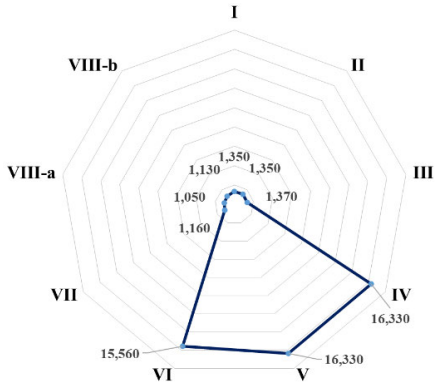

FIGURE 16. **$THD_{I_{output}}$-States.**

are systematically presented in Figures 16-18. This analysis serves as a comprehensive comparison of the different techniques across different states.

The single-phase 5-level HBNPC inverter system represents a complex yet highly efficient system. When we use SPWM, SV-PWM, and MPWM techniques, namely States I-III, VII, VIII-a, and VIII-b, we can confidently ensure that the load current THD value remains within the specified

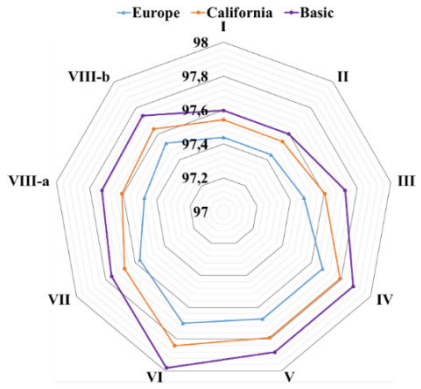

FIGURE 17. Efficiency-States.

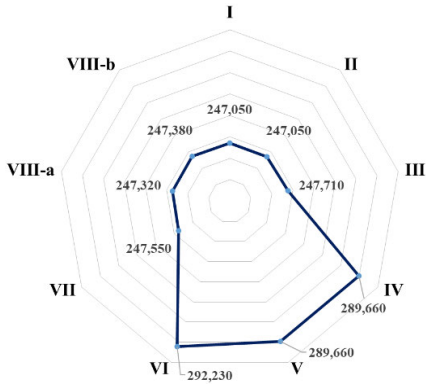

FIGURE 18. Output voltage ($V_{output}(V_{rms})$)-States.

5% limit value. This adherence to the standard is clearly outlined in Figure 16 of the standards [52], confirming that we meet the desired condition. However, one needs to be cautious when the THI-PWM technique is applied, encompassing States IV, V, and VI. In these instances, the observed THD values significantly surpass the standard limit, which could potentially lead to operational inefficiencies.

Taking a closer look at the system's performance, we find that the lowest three load current THD values were achieved using the MPWM and SV-PWM techniques. These results correspond to States VIII-a, VIII-b, and VII, respectively. These findings indicate the robust nature of these techniques in maintaining optimal system performance. However, the highest THD value was observed when employing the THI-PWM modulation technique, particularly in States IV, V, and VI. This suggests a need for further refinement when using this technique.

In terms of efficiency, Figure 17 provides a compelling illustration. State VI, which employs the THI-PWM modulation technique with a triangle signal type, displays superior performance. This superiority is measured in terms of Inverter Efficiency (η), European efficiency (η_{Europe}), and California efficiency ($\eta_{California}$). These results demonstrate the potential of the THI-PWM modulation technique when applied correctly. Additionally, Figure 18 presents a comprehensive view of the inverter output voltage ($V^*_{ouput}(V_{rms})$). It's notable that States VI, I, and II recorded the highest and lowest values, showcasing the broad range of performance within the system.

As depicted in Figure 19, within the linear modulation range ($m_{index} < 1$), it was observed that the THD value decreases with an increase in the modulation index. This implies that within this range, an increase in the modulation index can effectively reduce the distortion in the system. However, when we moved to the overmodulation range, we observed a different pattern. Within the overmodulation range ($m_{index} > 1$), it was determined that the THD value increases with an increase in the modulation index. This shows that beyond the linear range, an increase in the modulation index can lead to a significant increase in system distortion. Furthermore, it was noted that the THD value decreases with an increase in the switching frequency. This suggests that increasing the switching frequency can be an effective strategy to reduce the overall distortion in the system.

To illustrate the relationship between the modulation index (m_{index}), switching frequency (f_{sw}), and THD more precisely for a specific modulation technique, Figure 20 presents a detailed depiction.

As shown in Figure 20, there is a general trend where increasing the switching frequency is correlated with a decrease in THD. This inverse relationship indicates that as the switching frequency increases, the THD tends to decrease. It is important to note, however, that the relationship is not linear and there is a particular threshold below which changes in the switching frequency (f_{sw}) do not significantly affect the THD. This threshold for the switching frequency was found to be 5 kHz. Beyond this value, further increases in the switching frequency do not result in significant changes in the THD. In addition, it was observed that above a specific modulation index value (m_{index}), which was found to be 1, the THD value remains relatively stable without any significant changes. This suggests that once the modulation index exceeds a value of 1, the THD is not notably affected by further increases in the modulation index.

The relationship between the modulation index (m_{index}) and THD varies depending on the modulation technique at a given switching frequency (f_{sw}), as does the relationship between the modulation index (m_{index}) and converter output voltage (V_{output}). Additionally, the relationship between switching frequency and THD is influenced by the modulation index value. These intricate relationships are further elucidated in Figures 21-23.

Figure 21 clearly showcases that for States I, II, III, VII, VIII-a, and VIII-b, which employ the SPWM, SV-PWM, and MPWM modulation techniques, there is a noticeable decrease in THD as the modulation index increases within the linear modulation range, where the modulation index is less than 1 ($m_{index} < 1$). This is an important observation as it may influence the choice of modulation technique in certain applications. On the flip side, in the overmodulation range

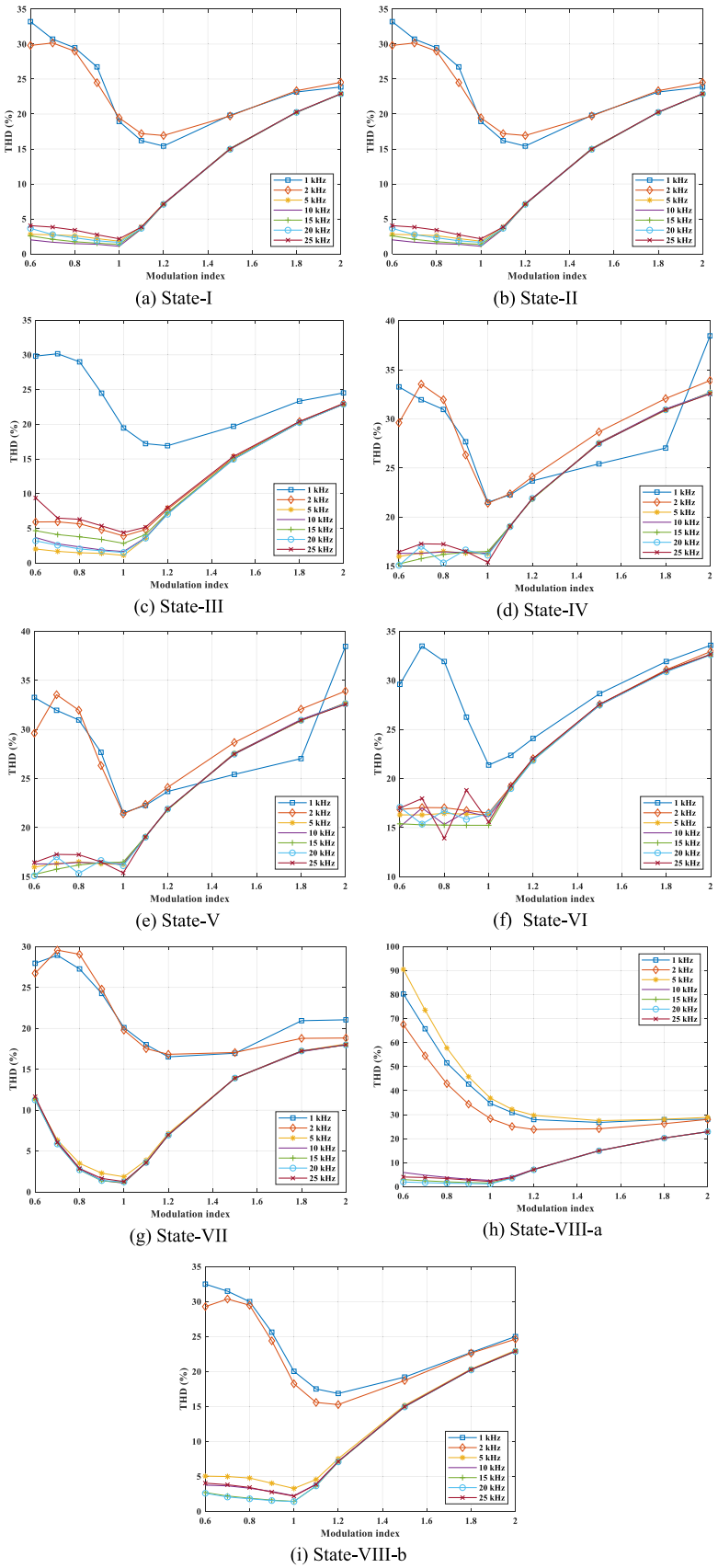

FIGURE 19. THD-m_{indeks}.

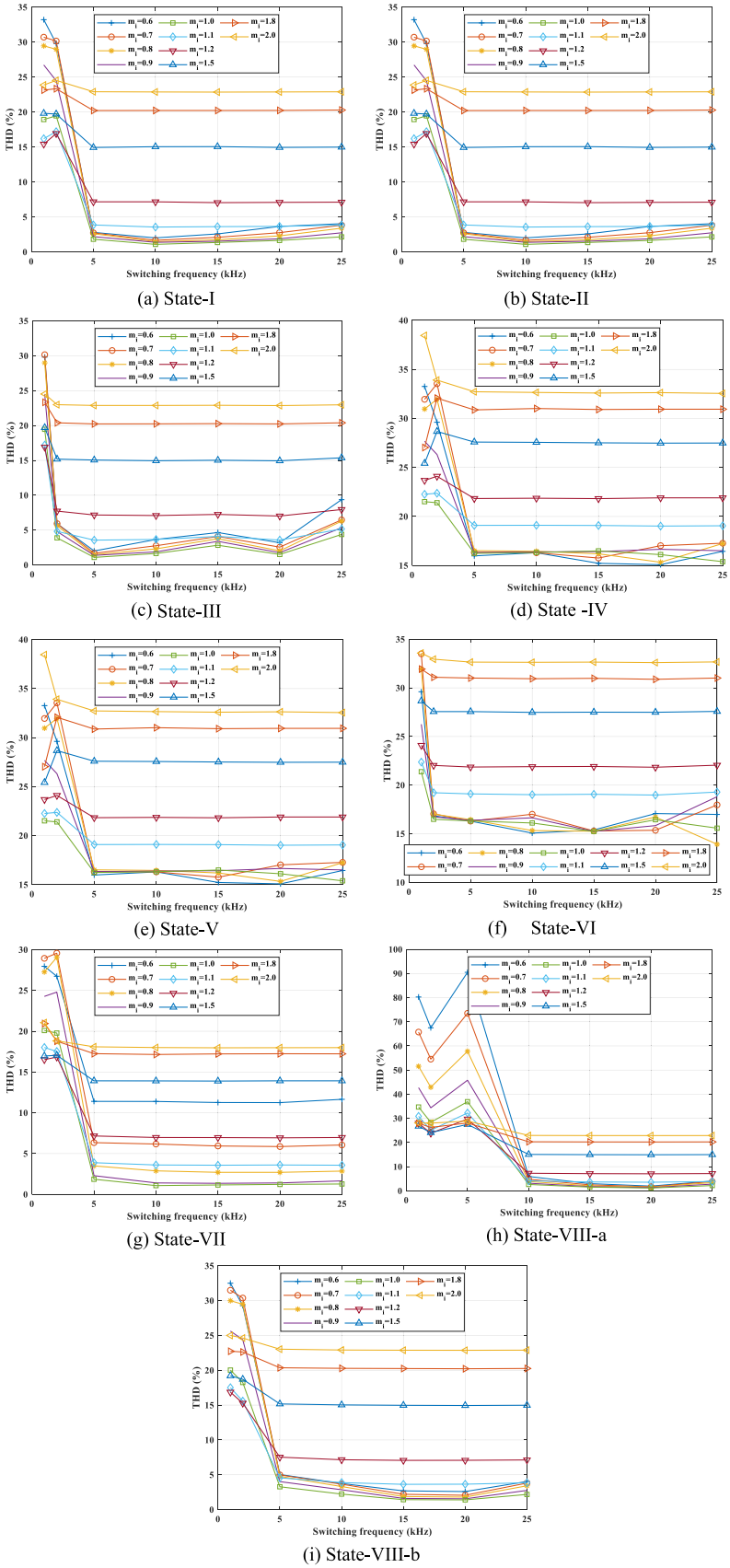

(a) State-I (b) State-II

(c) State-III (d) State -IV

(e) State-V (f) State-VI

(g) State-VII (h) State-VIII-a

(i) State-VIII-b

FIGURE 20. THD-f_{sw}.

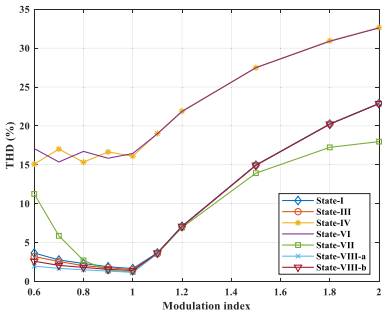

FIGURE 21. THD−m_{index} (f_{sw} = 20kHz).

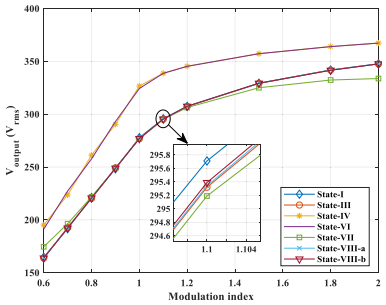

FIGURE 22. V_{output}−m_{index} (f_{sw} = 20kHz).

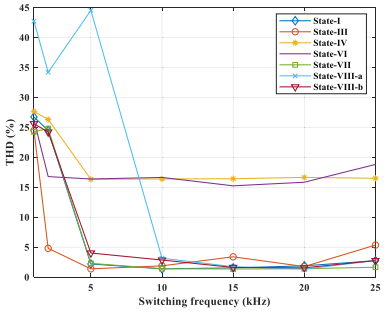

FIGURE 23. THD−f_{sw} (m_{index} = 0.9).

where the modulation index is greater than 1 ($m_{index} > 1$), there is an inverse relationship with the THD actually increasing as the modulation index rises. This highlights the potential challenges that can arise in the overmodulation range.

As for States IV, V, and VI, which utilize the less common THI-PWM technique, the THD doesn't follow a consistent pattern with the modulation index within the linear modulation range and overmodulation range. Instead, it exhibits varying trends, suggesting a more complex relationship that warrants further investigation.

Turning to the discussion on the fundamental switching frequency, Figure 22 provides a clear depiction of how the inverter's nominal output voltage (V_{output}) is directly tied to the modulation index (m_{index}) value. Specifically, as the modulation index value increases, so too does the inverter's nominal output voltage. This linear relationship is a key characteristic of the inverter's operation.

Lastly, Figure 23 offers an insight into the effect of the switching frequency on THD. It demonstrates that increasing the switching frequency (f_{sw}), generally leads to a decrease in THD when the modulation index value (m_{indeks}) is held at a constant 0.9. Nevertheless, there is an interesting caveat to this trend. When the switching frequencies surpass the fundamental frequency, specifically when it reaches 20 kHz (f_{sw} = 20kHz), the THD tends to increase, countering the previous trend. This suggests a limit to the benefits of increasing the switching frequency and highlights the need for careful frequency selection.

IV. CONCLUSION

This detailed study embarks on a comprehensive simulation of the single-phase 5-level HBNPC inverter topology. It leverages a variety of modulation techniques in MATLAB/Simulink for standalone operation modes. The in-depth simulation results encapsulate key aspects including the output voltage, the waveform of the output current, and the intricate relationships between efficiency-power and THD-power for different modulation types. The study meticulously examines results obtained from various modulation techniques such as SPWM, THI-PWM, SV-PWM, and MPWM, in conjunction with diverse carrier signal types. The findings are systematically presented in both tabular and graphical formats to aid in clear understanding and interpretation.

On a closer look at the simulation, it is revealed that in scenarios operating independently of the network using the THI-PWM technique, the THD values unfortunately exceed the 5% threshold specified in the standard. This happens in all cases except when operating at maximum power, where the THD values commendably fall below the threshold. Moreover, upon observation, a trend is noticed where efficiency tends to decrease as power decreases. Simultaneously, total harmonic distortion gradually increases across all operating conditions, indicating the intricate balance between these key factors in the operation of the inverter topology.

Moving forward, for studies involving PV systems utilizing PWM inverters, the following recommendations are suggested:

- The path towards achieving a more efficient and effective system, regardless of whether it is connected to the grid or operates as a standalone unit, can be significantly facilitated by making strategic adjustments such as reducing the number of switching elements present in the diode-clamped inverter.
- A thorough and careful consideration of various multilevel inverter types, viewed as potential alternatives to the more traditional diode-clamped inverter, holds the substantial potential to not only increase overall efficiency but also to decrease the THD.
- One of the proven tactics to enhance system performance is to increase the number of levels in the inverter. This strategy can contribute to minimizing filter requirements, thereby gradually shifting the output voltage

waveform towards a more sinusoidal shape and significantly reducing harmonics in the process.

- The exploration and development of new, innovative, and modified modulation techniques, by effectively leveraging existing strategies and insights gleaned from literature, presents promising and exciting avenues for improving the performance of the inverter system.
- By conducting a detailed and systematic analysis of system operation through variations in control methods, we have the opportunity to gain valuable insights into how we can optimize system efficiency and stability. This can potentially lead to the development of best practices for managing and operating inverter systems.
- Considering the three categories that can be named (topological improvement, considering new modulation technique, and using appropriate control strategies) to increase the efficiency of a power electronics converter system, reduce the harmonic distortions it causes, and meet the requirements of standards, it is important to conduct studies.

REFERENCES

[1] M. Ertem, "Renewable energy-aware machine scheduling under intermittent energy supply," *IEEE Access*, vol. 12, pp. 23613–23625, 2024, doi: 10.1109/ACCESS.2024.3365074.

[2] F. Z. Peng, C.-C. Liu, Y. Li, A. K. Jain, and D. Vinnikov, "Envisioning the future renewable and resilient energy grids—A power grid revolution enabled by renewables, energy storage, and energy electronics," *IEEE J. Emerg. Sel. Topics Ind. Electron.*, vol. 5, no. 1, pp. 8–26, Jan. 2024, doi: 10.1109/JESTIE.2023.3343291.

[3] D. Mazumdar, P. K. Biswas, C. Sain, and T. S. Ustun, "GAO optimized sliding mode based reconfigurable step size Pb&O MPPT controller with grid integrated EV charging station," *IEEE Access*, vol. 12, pp. 10608–10620, 2024, doi: 10.1109/ACCESS.2023.3344275.

[4] C.-H. Lin, M. S. Khan, J. Ahmad, H.-D. Liu, and T.-C. Hsiao, "Design and analysis of novel high-gain boost converter for renewable energy systems (RES)," *IEEE Access*, vol. 12, pp. 24262–24273, 2024, doi: 10.1109/ACCESS.2024.3365705.

[5] A. Rajamallaiah, S. P. K. Karri, M. L. Alghaythi, and M. S. Alshammari, "Deep reinforcement learning based control of a grid connected inverter with LCL-filter for renewable solar applications," *IEEE Access*, vol. 12, pp. 22278–22295, 2024, doi: 10.1109/ACCESS.2024.3364058.

[6] T. Mahmud and H. Gao, "A comprehensive review on matrix-integrated single-stage isolated MF/HF converters," *Electronics*, vol. 13, no. 1, p. 237, Jan. 2024, doi: 10.3390/electronics13010237.

[7] D. Mathew and R. C. Naidu, "A review on single-phase boost inverter technology for low power grid integrated solar PV applications," *Ain Shams Eng. J.*, vol. 15, no. 2, Feb. 2024, Art. no. 102365, doi: 10.1016/j.asej.2023.102365.

[8] J. Jiang, H. Wu, C. Zhong, Y. Cai, and H. Song, "A novel methodology for microgrid power quality disturbance classification using URPM-CWT and multi-channel feature fusion," *IEEE Access*, vol. 12, pp. 35597–35611, 2024, doi: 10.1109/access.2024.3350170.

[9] E. C. Resende, M. G. Simoes, and L. C. G. Freitas, "Anti-islanding techniques for integration of inverter-based distributed energy resources to the electric power system," *IEEE Access*, vol. 12, pp. 17195–17230, 2024, doi: 10.1109/ACCESS.2024.3357710.

[10] C. Roy, T. Bhattacharya, and D. Chatterjee, "Increase of effective switching frequency of parallel connected two-level inverters in high voltage STATCOM application using a current based reduced sorting algorithm," *IEEE Trans. Ind. Appl.*, vol. 60, no. 1, pp. 719–729, Jan/Feb. 2024, doi: 10.1109/TIA.2023.3327695.

[11] S. A. Saleh, "Maximum resolution based method for balancing capacitor voltages in 7-level single phase flying-capacitor wavelet modulated inverters," *IEEE Trans. Ind. Appl.*, vol. 59, no. 4, pp. 5019–5031, Jul. 2023, doi: 10.1109/TIA.2023.3258425.

[12] C. Qin, X. Li, C. Hou, and C. Su, "A fast-processing implementation method of virtual space vector modulation for the impedance-source three-level inverter," *IEEE Trans. Circuits Syst. II, Exp. Briefs*, early access, Feb. 5, 2024, doi: 10.1109/TCSII.2024.3362336.

[13] R. Kumar, B. Singh, and P. Kant, "Design and analysis of a 54-pulse converter and 7-level hybrid inverter for medium voltage induction motor drive," *IEEE Trans. Ind. Appl.*, vol. 60, no. 1, pp. 560–572, Jan./Feb. 2024, doi: 10.1109/TIA.2023.3313594.

[14] X. Zhao, C.-W. Chang, R. Phukan, R. Burgos, S. Uicich, P. Asfaux, and D. Dong, "An enhanced modulation scheme for multi-level T-type inverter with loss balance and reduction," *IEEE Trans. Power Electron.*, vol. 38, no. 11, pp. 14050–14064, Nov. 2023, doi: 10.1109/TPEL.2023.3289508.

[15] G. Rohner, T. Gfrörer, P. S. Niklaus, D. Bortis, M. Schweizer, and J. W. Kolar, "Comparative evaluation of three-phase three-level GaN and seven-level Si flying capacitor inverters for integrated motor drives considering overload operation," *IEEE Access*, vol. 12, pp. 7356–7371, 2024, doi: 10.1109/ACCESS.2024.3350728.

[16] M. Ye, W. Ren, L. Chen, Q. Wei, G. Song, and S. Li, "Research on power-balance control strategy of CHB multilevel inverter based on TPWM," *IEEE Access*, vol. 7, pp. 157226–157240, 2019, doi: 10.1109/ACCESS.2019.2950064.

[17] H. Yang, Z. Cheng, X. Zhang, and T. Yang, "A modulation strategy to operate five-level HC inverter at wide power factors with enhanced neutral point voltage balancing capability," *IEEE Trans. Power Electron.*, vol. 39, no. 1, pp. 744–767, Jan. 2024, doi: 10.1109/TPEL.2023.3322413.

[18] N. H. Charan, A. Bandyopadhyay, P. Roy, M. A. Babita, and M. S. Prabhu, "A single-phase cascaded H-bridge multilevel inverter with voltage boost ability: Modulation and analysis," *IEEE Trans. Ind. Appl.*, early access, Jan. 11, 2024, doi: 10.1109/tia.2024.3351796.

[19] D. Zakzewski, R. Resalayyan, and A. Khaligh, "Hybrid neutral point clamped converter: Review and comparison to traditional topologies," *IEEE Trans. Transport. Electrific.*, early access, Dec. 29, 2023, doi: 10.1109/TTE.2023.3348241.

[20] J. S. M. Ali, A. R. Khan, G. N. Pandurangan, P. Ponnusamy, F. S. Alamri, and S. A. Bahaj, "A 7L and 11L high step-up SCMLI topology with reduced component voltage stress," *IEEE Access*, vol. 11, pp. 139785–139797, 2023, doi: 10.1109/ACCESS.2023.3333363.

[21] M.-S. Song, J. Kim, and J.-B. Lee, "Full-bridge diode-clamped four-level symmetric switching converter," *IEEE Access*, vol. 11, pp. 103350–103363, 2023, doi: 10.1109/ACCESS.2023.3317432.

[22] A. Kokila and V. Senthil Kumar, "Design and analysis of dual output three level inverter with reduced switch count topology," *IETE J. Res.*, vol. 69, no. 1, pp. 567–583, Jan. 2023, doi: 10.1080/03772063.2020.1838339.

[23] A. Edpuganti and A. K. Rathore, "Optimal low-switching frequency pulsewidth modulation of medium voltage seven-level cascade-5/3H inverter," *IEEE Trans. Power Electron.*, vol. 30, no. 1, pp. 496–503, Jan. 2015, doi: 10.1109/TPEL.2014.2313552.

[24] B.-R. Lin and C.-H. Huang, "Implementation of a three-phase capacitor-clamped active power filter under unbalanced condition," *IEEE Trans. Ind. Electron.*, vol. 53, no. 5, pp. 1621–1630, Oct. 2006, doi: 10.1109/TIE.2006.881991.

[25] J. Rodriguez, J.-S. Lai, and F. Zheng Peng, "Multilevel inverters: A survey of topologies, controls, and applications," *IEEE Trans. Ind. Electron.*, vol. 49, no. 4, pp. 724–738, Aug. 2002, doi: 10.1109/TIE.2002.801052.

[26] P. Kumar and P. Singhal, "Multilevel inverter topologies with various PWM firing sequences," in *Proc. 1st Int. Conf. Cyber Phys. Syst., Power Electron. Electric Vehicles (ICPEEV)*, Hyderabad, India, Sep. 2023, pp. 1–7, doi: 10.1109/icpeev58650.2023.10391845.

[27] A. M. Mahfuz-Ur-Rahman, Md. R. Islam, K. M. Muttaqi, and D. Sutanto, "Model predictive control for a new magnetic linked multilevel inverter to integrate solar photovoltaic systems with the power grids," *IEEE Trans. Ind. Appl.*, vol. 56, no. 6, pp. 7145–7155, Nov. 2020, doi: 10.1109/TIA.2020.3024352.

[28] A. Lewicki, C. Odeh, and M. Morawiec, "Space vector pulsewidth modulation strategy for multilevel cascaded H-bridge inverter with DC-link voltage balancing ability," *IEEE Trans. Ind. Electron.*, vol. 70, no. 2, pp. 1161–1170, Feb. 2023, doi: 10.1109/TIE.2022.3158005.

[29] J. Tanguturi and S. Keerthipati, "Power balancing strategy for cascaded H-bridge inverter in a grid-connected photovoltaic system under asymmetrical operating conditions," *IEEE Trans. Ind. Electron.*, vol. 71, no. 6, pp. 5853–5862, Jun. 2024, doi: 10.1109/TIE.2023.3292869.

[30] S. J. Lim, S.-P. Kim, F.-S. Kang, and S.-G. Song, "Reliability analysis based on Markov model, economic feasibility, and efficiency comparison for a cascaded H-bridge multilevel inverter capable of generating 27 levels," *IEEE Access*, vol. 12, pp. 21530–21542, 2024, doi: 10.1109/ACCESS.2024.3363832.

[31] Z. A. Alqarni, "Design of active fault-tolerant control system for multilevel inverters to achieve greater reliability with improved power quality," *IEEE Access*, vol. 10, pp. 77791–77801, 2022, doi: 10.1109/ACCESS.2022.3193790.

[32] M. Paramasivan, K. Eswaramoorthy, R. Muniraj, P. L. Kanthan, T. S. Babu, S. Jeevananthan, and H. H. Alhelou, "An alternative level enhanced switching angle modulation schemes for cascaded H bridge multilevel inverters," *IEEE Access*, vol. 11, pp. 57365–57382, 2023, doi: 10.1109/ACCESS.2023.3283253.

[33] R. Xie, Q. Zeng, F. Yang, B. Lin, O. Xu, and Y. He, "Decoupled unipolar hysteresis current control for single-phase grid-tied inverter without current zero-crossing distortion," *IEEE Access*, vol. 12, pp. 21453–21463, 2024, doi: 10.1109/ACCESS.2024.3359456.

[34] Y. Lyu, Y. Zi, and X. Li, "Improved control of capacitor voltage balancing in modular multilevel converter submodules," *IEEE Access*, vol. 12, pp. 19510–19519, 2024, doi: 10.1109/ACCESS.2024.3350178.

[35] S. Nyamathulla, D. Chittathuru, and S. M. Muyeen, "An overview of multilevel inverters lifetime assessment for grid-connected solar photovoltaic applications," *Electronics*, vol. 12, no. 8, p. 1944, Apr. 2023, doi: 10.3390/electronics12081944.

[36] S. Nyamathulla and D. Chittathuru, "A review of multilevel inverter topologies for grid-connected sustainable solar photovoltaic systems," *Sustainability*, vol. 15, no. 18, p. 13376, Sep. 2023, doi: 10.3390/su151813376.

[37] Z. Dong and C. Liu, "Three-dimension space vector modulation for three-phase series-end winding voltage-source inverters," *IEEE Trans. Ind. Electron.*, vol. 71, no. 1, pp. 82–92, Jan. 2024, doi: 10.1109/TIE.2023.3241399.

[38] A. J. Memon, M. A. Mahar, A. S. Larik, and M. M. Shaikh, "A comprehensive review of reduced device count multilevel inverters for PV systems," *Energies*, vol. 16, no. 15, p. 5638, Jul. 2023, doi: 10.3390/en16155638.

[39] S. P. Sunddararaj, S. S. Rangarajan, and N. Subashini, "An extensive review of multilevel inverters based on their multifaceted structural configuration, triggering methods and applications," *Electronics*, vol. 9, no. 3, p. 433, Mar. 2020, doi: 10.3390/electronics9030433.

[40] S. Arazm, H. Vahedi, and K. Al-Haddad, "Generalized phase-shift pulse width modulation for multi-level converters," in *Proc. IEEE Electr. Power Energy Conf. (EPEC)*, Toronto, ON, Canada, Oct. 2018, pp. 1–6, doi: 10.1109/EPEC.2018.8598340.

[41] S. Kouro, M. Malinowski, K. Gopakumar, J. Pou, L. G. Franquelo, B. Wu, J. Rodriguez, M. A. Pérez, and J. I. Leon, "Recent advances and industrial applications of multilevel converters," *IEEE Trans. Ind. Electron.*, vol. 57, no. 8, pp. 2553–2580, Aug. 2010, doi: 10.1109/TIE.2010.2049719.

[42] F. Faraji and H. Cha, "Paralleled H-bridge multilevel switching-cell current source inverter," *IEEE Trans. Power Electron.*, vol. 39, no. 5, pp. 5793–5805, May 2024, doi: 10.1109/TPEL.2024.3367372.

[43] D. G. Holmes and T. A. Lipo, *Pulse Width Modulation for Power Converters: Principles and Practice*. USA: Wiley, 2003, doi: 10.1109/9780470546284.

[44] N. I. Nahin, S. P. Biswas, S. Mondal, Md. R. Islam, and S. M. Muyeen, "A modified PWM strategy with an improved ANN based MPPT algorithm for solar PV fed NPC inverter driven induction motor drives," *IEEE Access*, vol. 11, pp. 70960–70976, 2023, doi: 10.1109/ACCESS.2023.3291339.

[45] A. Ruiz-Gonzalez, J.-R. Heredia-Larrubia, M. J. Meco-Gutierrez, and F.-M. Perez-Hidalgo, "Pulse-width modulation technique with harmonic injection in the modulating wave and discontinuous frequency modulation for the carrier wave for multilevel inverters: An application to the reduction of acoustic noise in induction motors," *IEEE Access*, vol. 11, pp. 40579–40590, 2023, doi: 10.1109/ACCESS.2023.3269593.

[46] J.-S. Lee, S.-J. Lee, and K.-B. Lee, "Novel switching method for single-phase NPC three-level inverter with neutral-point voltage control," *Int. J. Electron.*, vol. 105, no. 2, pp. 303–323, Feb. 2018, doi: 10.1080/00207217.2017.1357202.

[47] T. E. Shults, O. Husev, F. Blaabjerg, C. Roncero-Clemente, E. Romero-Cadaval, and D. Vinnikov, "Novel space vector pulsewidth modulation strategies for single-phase three-level NPC impedance-source inverters," *IEEE Trans. Power Electron.*, vol. 34, no. 5, pp. 4820–4830, May 2019, doi: 10.1109/TPEL.2018.2859194.

[48] J. Guzman-Guemez, D. S. Laila, and S. M. Sharkh, "State-space approach for modelling and control of a single-phase three-level NPC inverter with SVPWM," in *Proc. IEEE Power Energy Soc. Gen. Meeting (PESGM)*, Boston, MA, USA, Jul. 2016, pp. 1–5, doi: 10.1109/PESGM.2016.7741355.

[49] L. Kefeng, X. Fei, L. Jilong, M. Zhiqin, and D. Zhuangzhi, "An asymmetrical active-neutral-point-clamped five-level H-bridge inverter for open-winding motor applications with its modulation strategy," *IEEE Trans. Power Electron.*, vol. 38, no. 10, pp. 12010–12023, Oct. 2023, doi: 10.1109/TPEL.2023.3276795.

[50] N. Vaishnav and A. K. Jain, "Reactive power flow in induction motor drive with inverter output sinusoidal filter and its influence on wide frequency operation," *IEEE Trans. Energy Convers.*, vol. 38, no. 2, pp. 1073–1084, Jun. 2023, doi: 10.1109/TEC.2022.3229111.

[51] K.-S. Kim, S.-G. Jeong, O. Kwon, and B.-H. Kwon, "Weighted efficiency enhancement for single-power-conversion microinverters using hybrid-mode modulation strategy," *IEEE Trans. Ind. Electron.*, vol. 67, no. 12, pp. 10243–10252, Dec. 2020, doi: 10.1109/TIE.2019.2962484.

[52] *IEEE Approved Draft Application Guide for IEEE Std 1547, IEEE Standard for Interconnecting Distributed Resources With Electric Power Systems*, Standard IEEE P1547.2/D6.5, Aug. 2023.

NAZLICAN CAVLI received the B.Sc.E. degree in electrical and electronics engineering and the M.Sc.E. degree in electrical engineering from Karadeniz Technical University (KTU), Trabzon, Türkiye, in 2019 and 2021, respectively, where she is currently pursuing the Ph.D. degree in electrical and electronic engineering. She is also a Lecturer with the Department of Electrical and Energy, Tercan Vocational School, Erzincan Binali Yıldırım University, Erzincan, Türkiye. She completed her primary and secondary education in Kars.

EMRE OZKOP (Senior Member, IEEE) received the B.Sc.E. degree in electrical and electronics engineering from Gazi University, Ankara, Türkiye, in 2003, and the M.Sc.E. and Ph.D. degrees in electrical engineering from Karadeniz Technical University (KTU), Trabzon, Türkiye, in 2006 and 2012, respectively. He is currently an Associate Professor with the Department of Electrical and Electronics Engineering, KTU. His research interests include power electronics, intelligent control systems, protection and grounding systems, renewable energy systems operation, control and protection, and smart grids.